

## ULTRA-WIDEBAND DIELECTRIC-LOADED HORN ANTENNA WITH DUAL-LINEAR POLARIZATION CAPABILITY

J.-Y. Chung

Department of Electrical and Computer Engineering  
The Ohio State University  
1320 Kinnear Road, OH 43212, USA

**Abstract**—In order to improve measurement efficiency in electromagnetic test facilities (compact range or near-field range), testing probes are required to have ultra-wideband (UWB) radiation characteristics, dual-polarization capability, and interchangeable  $E$ - and  $H$ -plane far-field patterns. In this context, we propose a new type of UWB antenna that satisfies these requirements in the frequency range of 4 to 18 GHz. For the proposed antenna, a low-loss dielectric material is loaded over pairs of balanced feeds to overcome radiation performance degradation addressed in purely metallic antennas. Also, radiation patterns are further improved by employing a lens aperture and shielding structures. The measured results of the final antenna design demonstrate broad and stable far-field patterns (half-power beamwidth  $> 45^\circ$ ), low voltage standing-wave ratio ( $< 2$ ), similar  $E$ - and  $H$ -plane patterns, and large cross-polarization isolation ( $> 23$  dB).

### 1. INTRODUCTION

Ultra-wide band (UWB) operation has become one of the most essential properties for antennas used in electromagnetic testing facilities (e.g., far-field or near-field test ranges), as it offers significant reduction in measurement effort/time. Moreover, if the antenna has dual polarization capability and interchangeable  $E$ - and  $H$ -plane patterns, the testing procedure can be further simplified since there is no need to mechanically rotate the antenna for different test configurations (e.g., cross-pol/co-pol and  $E$ -/ $H$ -plane measurements).

Typically, the operation bandwidth of UWB antennas is determined by the stability of antenna characteristics such as voltage

---

Corresponding author: J.-Y. Chung (chung.275@osu.edu).

standing-wave ratio (VSWR), gain, far-field radiation pattern, cross-pol isolation, etc. For antennas in testing facilities, the most important consideration is stable far-field radiation patterns. In particular, the antenna must maintain wide half-power beamwidth (HPBW) over a wide bandwidth to uniformly illuminate the reflector or the antenna under test. Such broad radiation patterns are also advantageous for the electromagnetic compatibility (EMC) test in that the electronic device can be adequately felled into the main-lobe.

The most widely used UWB antenna for the above objectives is the double-ridged horn antenna [1–6]. The double-ridged horn is simple in structure, easy to excite, and retain stable antenna gain and VSWR over a wide bandwidth (up to 18 : 1). The operation bandwidth of the double-ridged horn is commonly defined by its VSWR. However, there had been little concern regarding the far-field radiation patterns until the main-beam splitting problem (due to the higher-order mode propagation) was reported by Burns et al. [3]. Moreover, the double-ridged horn has large variations in beamwidth (e.g., HPBW varies from 30° to 60°) as well as large difference in  $E$ - and  $H$ -plane patterns since its body is mainly implemented with highly conductive materials.

In this context, many researchers have frequently employed dielectric materials to overcome shortcomings in metallic antennas [7, 8]. A good example of the efforts to resolve the radiation pattern issues in the double-ridged horn can be the UWB dielectric horn antenna developed by Lee et al. [9]. The antenna was built with a solid dielectric body so that the wave guiding mechanism is governed by soft dielectric-air boundaries instead of hard metallic walls. This also implies the main radiation source of the antenna is the dominant hybrid mode ( $HE_{11}$ ) having symmetric  $E$ - and  $H$ -field distributions [10, 11]. As a result, stable radiation characteristic with similar  $E$ - and  $H$ -plane patterns could be provided with this antenna. However, the antenna suffers from low efficiency (10–27%). Also, the bulk of the antenna, 7 inches (17.8 cm) in diameter and 4 inches (10.2 cm) in height, is unappealing.

In this paper, we propose a new UWB antenna combining beneficial features of the double-ridged horn and Lee's dielectric horn. Figure 1 illustrates the proposed dielectric-loaded horn. The primary goal of this antenna is to provide stable and broad far-field patterns (HPBW > 45°) over a wide frequency range (4–18 GHz). The exponentially tapered profile is inherited from the double-ridged horn to carry out broadband impedance transition and gradual radiation. Also, similar to Lee's dielectric horn, the antenna maintains axial symmetry and incorporates with a small amount of metallic fixtures to obtain broad and similar  $E$ - and  $H$ -plane patterns. The beamwidth is further optimized by integrating a spherical lens on the top.

Below, we first describe general antenna configurations in Section 2. In Section 3, studies on the exponential curve and lens aperture profiles to achieve broader antenna beamwidth are presented. Section 4 describes antenna shielding process by means of absorbers and conductive housing. Experiment results of the final design are shown in Section 5. These include VSWR, far-field patterns, co- and cross-pol gain, and radiation efficiency.

## 2. ANTENNA CONFIGURATION

As depicted in Fig. 1, the proposed antenna consists of an exponentially tapered dielectric body, spherical lens aperture, and metal plates. The antenna is fed by pairs of balanced coaxial cables [see the bottom of Fig. 1(a)]. Specifically, four coaxial cables are adjoined in  $90^\circ$  to each other, and two of each pair are responsible for exciting dual-linear polarized fields. The outer conductors of the coaxial cables are gradually tapered to realize broadband impedance transition from the

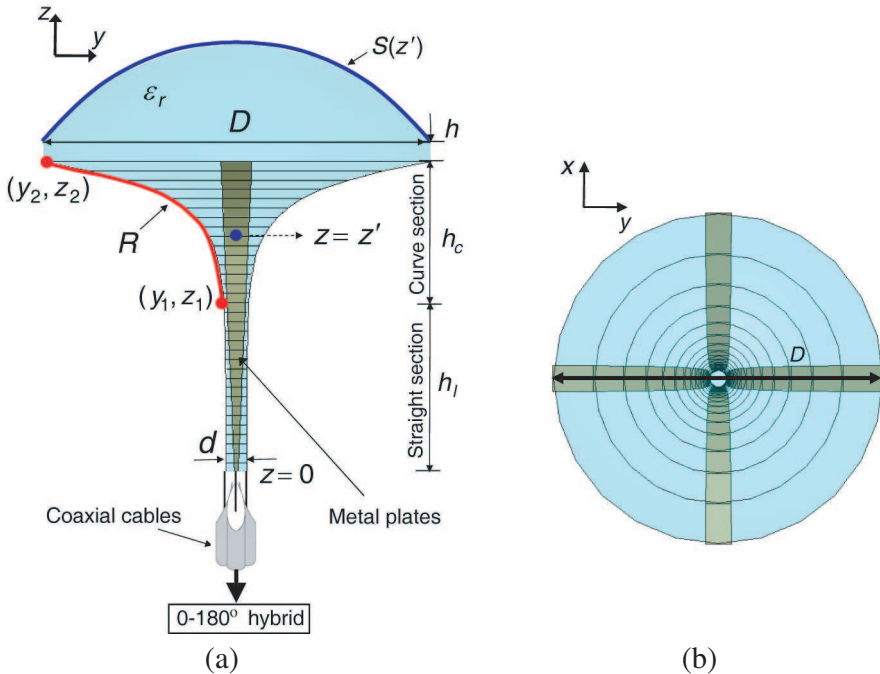


**Figure 1.** Geometry of the dielectric-loaded horn antenna: (a) Side-view and (b) top-view.

coaxial lines to the two-conductor transmission lines [12]. Noting that 0–180° hybrids are connected to the other ends of the cables as baluns.

Prior to the curve section, the straight section is located for a smooth impedance transition. It is found from simulations and measured data that the length of the straight section ( $h_s$ ) should be more than 2 times of the wavelength at high frequencies ( $> 14$  GHz) to maintain VSWR lower than 2. In our design, the straight section has a height of  $h_s = 1.75$  inches (4.5 cm) and width of  $d = 0.2$  inches (5 mm).

The body and aperture of the antenna are made of Acrylic (dielectric constant of  $\epsilon_r = 2.5$ , loss tangent of  $\tan \delta < 0.002$ ). The diameter of the aperture is set to  $D = 4$  inches (10.1 cm), which is larger than a wavelength at the lowest frequency (e.g.,  $\lambda_{4\text{GHz}} = 7.5$  cm). Also, we note that  $h = 0.2$  inches (5 mm) gap remains between the curve section and lens aperture to easily hold the antenna during fabrication. As the curve section and lens aperture are closely related to antenna's beamwidth, we discuss their designs in details in the next section.

### 3. ANTENNA BEAMWIDTH IMPROVEMENT

To achieve broad HPBW over a wide bandwidth, two parameters that significantly affect the antenna's far-field patterns are examined while other parameters are fixed as in Section 2.

#### 3.1. Opening Rate, $R$

The opening rate ( $R$ ) is a crucial design parameter that determines the curvature profile of exponentially tapered antennas such as transverse electromagnetic (TEM) horns [13, 14] and Vivaldi antennas [15–17]. It is given in the general curvature equation as below:

$$y = C_1 \exp(Rz) + C_2, \quad (1)$$

$$C_1 = \frac{y_2 - y_1}{\exp(Rz_2) - \exp(Rz_1)}, \quad (2)$$

$$C_2 = \frac{y_1 \exp(Rz_2) - y_2 \exp(Rz_1)}{\exp(Rz_2) - \exp(Rz_1)}, \quad (3)$$

where  $(y_1, z_1)$  and  $(y_2, z_2)$  refer to the starting and ending points of the curve section (see Fig. 1). As can be seen in Fig. 2,  $R$  determines the slope of the curve. For example, the slope becomes constant if  $R = 0$ , resulted in a linear profile. For a larger  $R$  value, the slope changes more abruptly along with the  $y$ - and  $z$ -axes. The height of the curve section is  $h_c = z_2 - z_1$ . It has been reported that the shorter

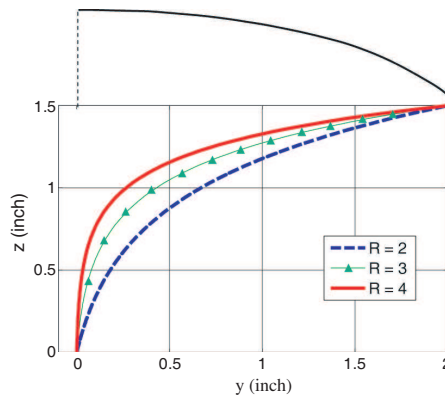


**Figure 2.** Curvature profile with different opening rates.

$h_c$  provides broader beamwidths [16], which agrees with our goal. However, if  $h_c$  were too short, it was observed that the main-lobe was distorted by strong diffraction from the end of metal arms, especially at lower frequencies ( $< 5$  GHz). Based on experimental studies, we chose  $h_c = 1.5$  inches (3.8 cm). With this value, the diffraction only impact the outside of the main-lobe (e.g.,  $\theta < -30^\circ$  and  $\theta > 30^\circ$ ).

Having determined  $h_c$ , we proceed to examine the impact of  $R$  on the antenna beamwidth using a full-wave simulation tool (Ansoft HFSS). Fig. 3 shows the simulated far-field patterns at different frequencies with  $R = 2, 3$ , and 4. For the low frequency [4 GHz, Fig. 3(a)], the beamwidth is hardly altered by  $R$  but sufficiently broad (HPBW  $> 70^\circ$ ). It is evident for the middle frequency [10 GHz, Fig. 3(b)] that the beamwidth increases as the curve section has more abruptly changing profile. However, no significant beamwidth broadening is observed for the high frequency as shown in Fig. 3(c). This is because the high frequency radiation mostly occurs at the beginning of the curved section. In general, the beamwidth resulting from such directly radiating fields can be controlled by adjusting the flare angle. However, this is not an option for antennas incorporating with abrupt curvature profiles. Instead, we adjust the lens aperture profile to improve the beamwidth.

### 3.2. Lens Aperture Profile, $S(z)$

The opportunity to shape the lens aperture offers another degree of freedom for the antenna beamwidth improvement. In tradition, lenses have been used to convert spherical wavefronts into planar ones to improve the antenna directivity [18, 19]. In opposition, the radiation

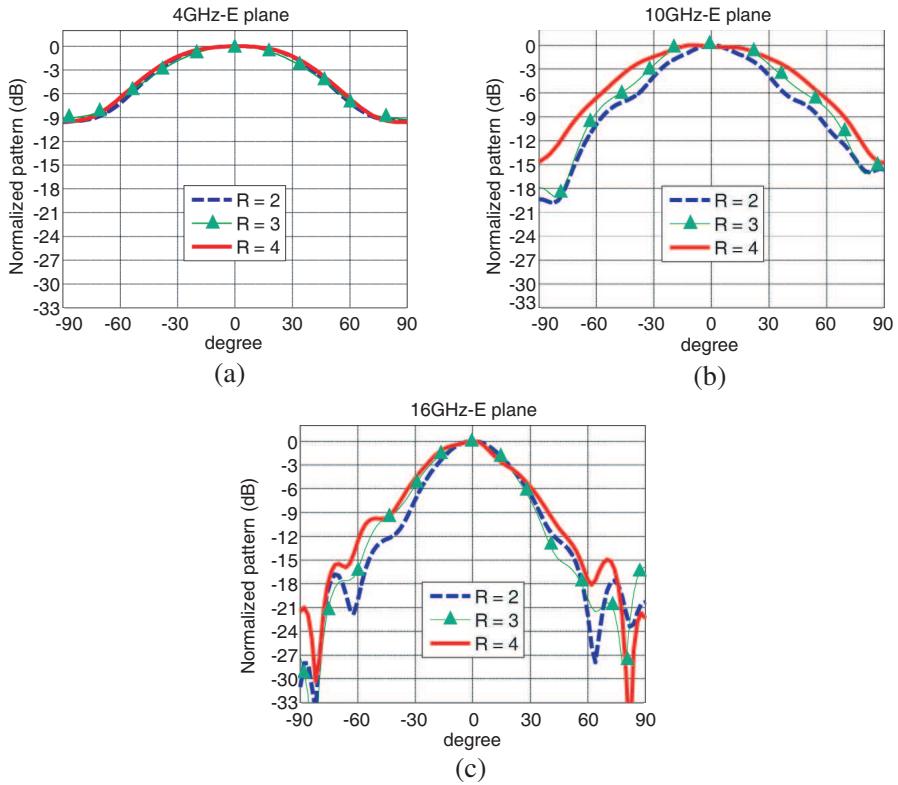


**Figure 3.** Simulated far-field patterns with different opening rates: (a) 4 GHz, (b) 10 GHz, and (c) 16 GHz.

pattern can be defocused (i.e., the beamwidth can be broaden) if the lens is designed to generate the phase front with more convexity. To demonstrate this, we compare the simulated phase data of two different lens profiles. Fig. 4(a) is the 2D phase plot when the center of the spherical aperture is located at 2.5 inches (6.35 cm) away from the feeding point, namely  $S(z = 2.5)$ . As observed, the phase front conforms to the dielectric-air boundary (black thick line) for this case. On the other hand, Fig. 4(b) is the phase plot when the phase front is intentionally mismatched against the dielectric-air boundary by locating the sphere center at 1.5 inches (3.81 cm), i.e.,  $S(z = 1.5)$ . It is clearly observed that the phase front leaving the dielectric-air boundary is much projecting outward when  $S(z = 1.5)$ . The HPBW's with these two lens profiles were calculated and illustrated in Fig. 5. This comparison shows that retreating the sphere center for 1 inch

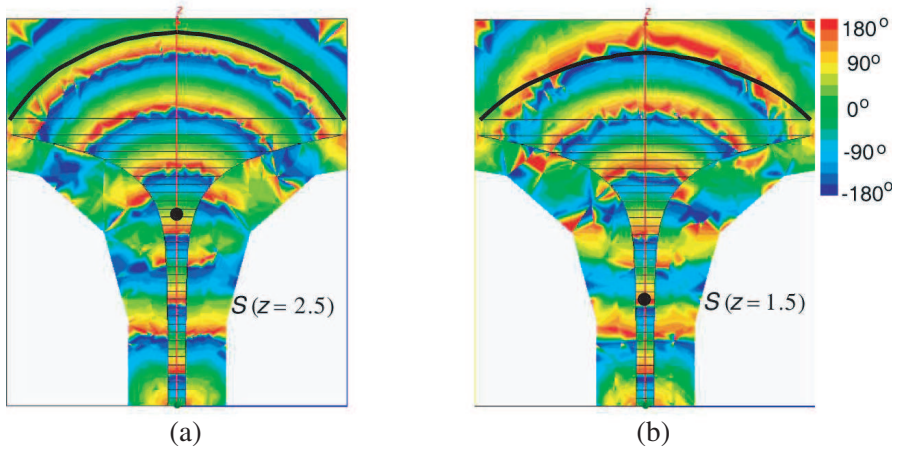


**Figure 4.** Simulated phase plots for (a)  $S(z = 2.5)$  and (b)  $S(z = 1.5)$ . The black dots and thick lines refer to the locations of sphere centers and dielectric-air boundaries.

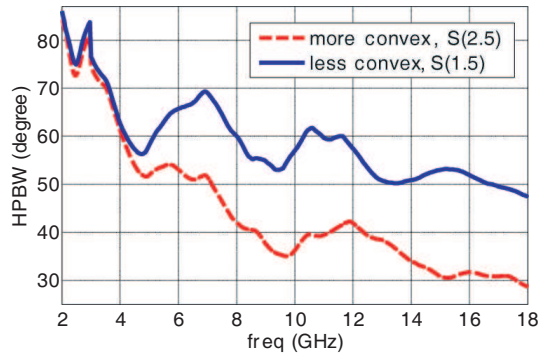


**Figure 5.** Half-power beamwidth comparison of antennas with two different lens profiles.

provides HPBW increment of 6 to 20° after 5 GHz. Consequently, the HPBW is more than 47° up to 18 GHz when the antenna is equipped with the  $S(z = 1.5)$  lens aperture.

#### 4. ANTENNA SHIELDING

A shielding structure is often required in UWB antenna design to reduce effects from stray signals, creeping waves, and leaky

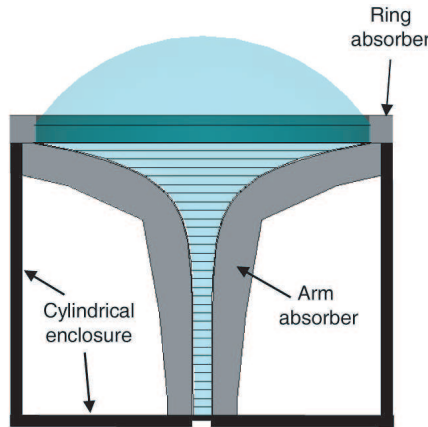


**Figure 6.** Antenna geometry with absorbers and conductive enclosure.

waves [9, 13, 20]. In common, radiation patterns at higher frequencies are more vulnerable to these undesirable effects. In the new dielectric-loaded antenna, microwave absorbers and conductive enclosure are used to attenuate them, as illustrated in Fig. 6. Absorbers are located at the outside of metal arms (arm absorber) and the circumference of the aperture (ring absorber). It is worth noting that such absorber treatment caused a maximum of 2 dB reduction in the measured antenna gain. However, applying absorbers at undesirable radiation sources is still worth for UWB antennas whose primary consideration is the well-behaved radiation patterns. Fig. 7 demonstrates the improvement in the measured far-field patterns at high frequencies (16 and 18 GHz). The ripples around the main-beams are suppressed when the absorbers are applied. Consequently, the radiation patterns have better continuity and symmetry.

Followed by the absorber treatment, the antenna is placed inside the cylindrical enclosure [4.5 inches (10.8 cm) in diameter and height]. This is particularly necessary for the testing antennas in electromagnetic facilities since any inadequate communication between the antenna and other equipments should be avoided. With appropriate shielding, which does not interfere with the main radiation sources, significant reduce of the side-lobe level can be achieved by blocking direct radiations from the feed and spill overs [21, 22]. Fig. 8 shows examples of the side-lobe level reduction at 5 and 10 GHz after shielding the antenna. Also noting that the front-to-back ratio is improved from approximately 20 dB to 35 dB by the shielding.

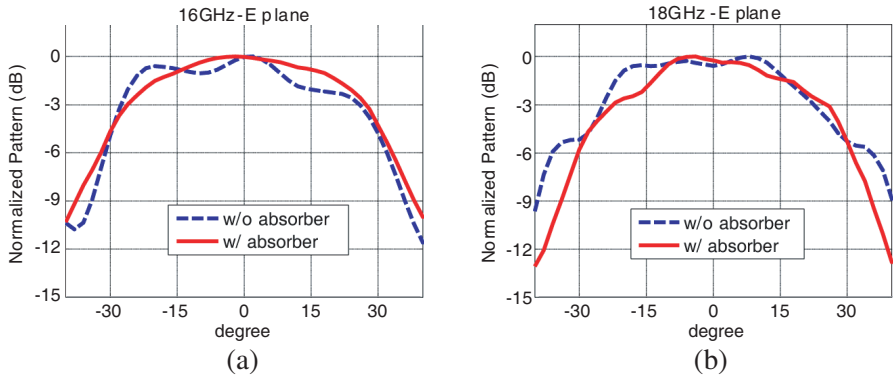


**Figure 7.** Main-beam pattern improvement after applying absorbers at (a) 16 GHz and (b) 18 GHz.

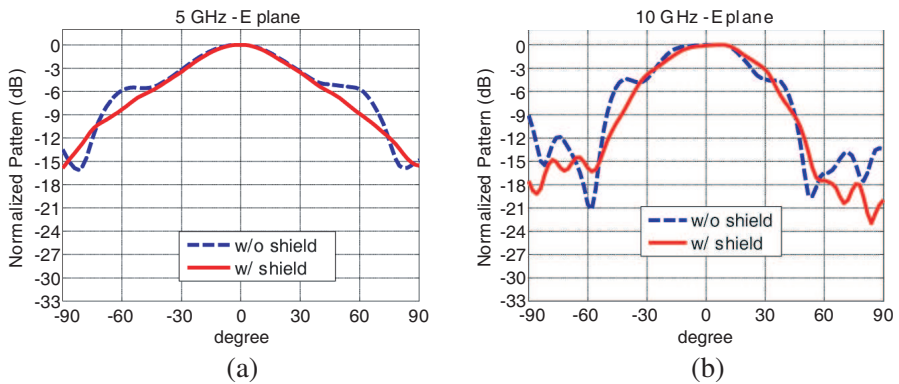


**Figure 8.** Side-lobe level reduction using shielding enclosure at (a) 5 GHz and (b) 10 GHz.

## 5. ANTENNA CHARACTERIZATION

In this section, we illustrate radiation performances of the dielectric-loaded antenna. The final design was carried out with  $R = 4$ ,  $S(z = 1.5)$ , and the parameters described in Section 2. Figs. 9(a) and (b) show the final design inserted in the shielding structure and mounted on OSU-ESL anechoic chamber for characterization.

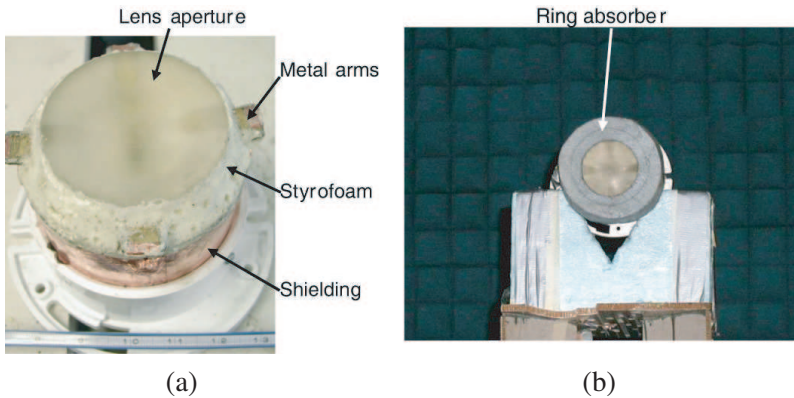


**Figure 9.** Fabricated dielectric-loaded horn (a) with shielding structure and (b) in anechoic chamber for testing.

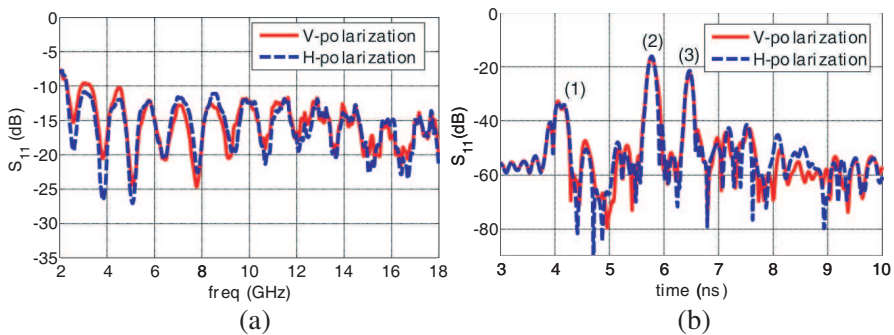


**Figure 10.** Measured  $S_{11}$  in (a) frequency domain and (b) time domain. The numbers in (b) refer to the responses from (1) 0–180° hybrid, (2) cable-antenna junction, and (3) aperture-air boundary.

### 5.1. Return Loss

Figures 10(a) and (b) show the measured return loss ( $S_{11}$ ) in the frequency and time domains, respectively. It is observed that the antenna has dual-linear polarization capability since the  $S_{11}$  data of vertically ( $V$ -pol) and horizontally ( $H$ -pol) fed antennas are in excellent agreement. Moreover,  $S_{11} < 10$  dB (VSWR  $< 2$ ) is achieved over the bandwidth of interest (4 to 18 GHz). The oscillatory behavior in the frequency domain [see Fig. 10(a)] is due to the interaction of two obvious peaks shown in the time domain plot [(2) and (3) in Fig. 10(b)]. These peaks correspond to the reflections at the coaxial cable-antenna

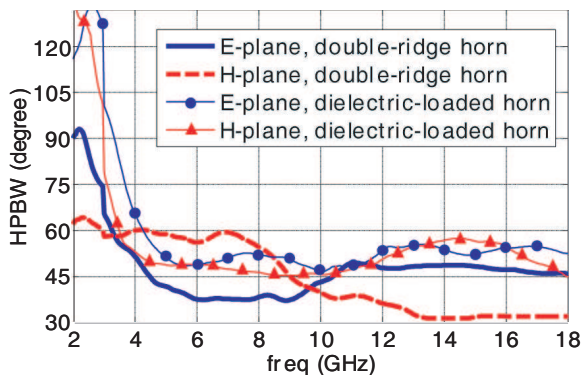


**Figure 11.** Comparison of measured half-power beamwidths of a double-ridged horn and the new dielectric-loaded horn antenna.

and aperture-air junctions. Otherwise, the peak (1) is resulted from the reflection inside the  $0\text{--}180^\circ$  hybrid. It was further observed that the peak (3) increases from  $-22.5$  to  $-16.8$  dB if the antenna is designed with  $\epsilon_r = 4$  dielectric material instead of  $\epsilon_r = 2.5$ .

## 5.2. HPBW and Far-field Pattern

The measured HPBWs of the new dielectric-loaded horn and a conventional double-ridged horn are compared in Fig. 11. As observed, the HPBWs of *E*- and *H*-planes for the double-ridged horn exhibit opposite trends in the low and high frequency ranges. Specifically, the *E*-plane HPBW is more than  $45^\circ$  above 11 GHz but less than  $40^\circ$  below 7 GHz. For the *H*-plane, this difference is more obvious (varies from  $31^\circ$  to  $60^\circ$ ). Such differences in HPBWs are due to the different guiding and radiation mechanisms for the *E*- and *H*-fields on the metallic ridges. On the other hand, the HPBWs of the dielectric-loaded horn show relatively small variations after 4 GHz as well as similar *E*- and *H*-plane patterns. This can be more clearly observed in Figs. 12(a), (b), and (c) illustrating the *E*- and *H*-plane far-field patterns of 4, 12, and 18 GHz. As can be seen, the *E*- and *H*-plane patterns are similar to each other at the broad main-lobes.

## 5.3. Antenna Gain and Radiation Efficiency

Figure 13 shows the co- and cross-polarization gains of the dielectric-loaded horn. As observed, the co-pol gain increases from 0 to 8.9 dBi in the range of 4 to 18 GHz. Furthermore, a minimum of 23 dB cross-pol

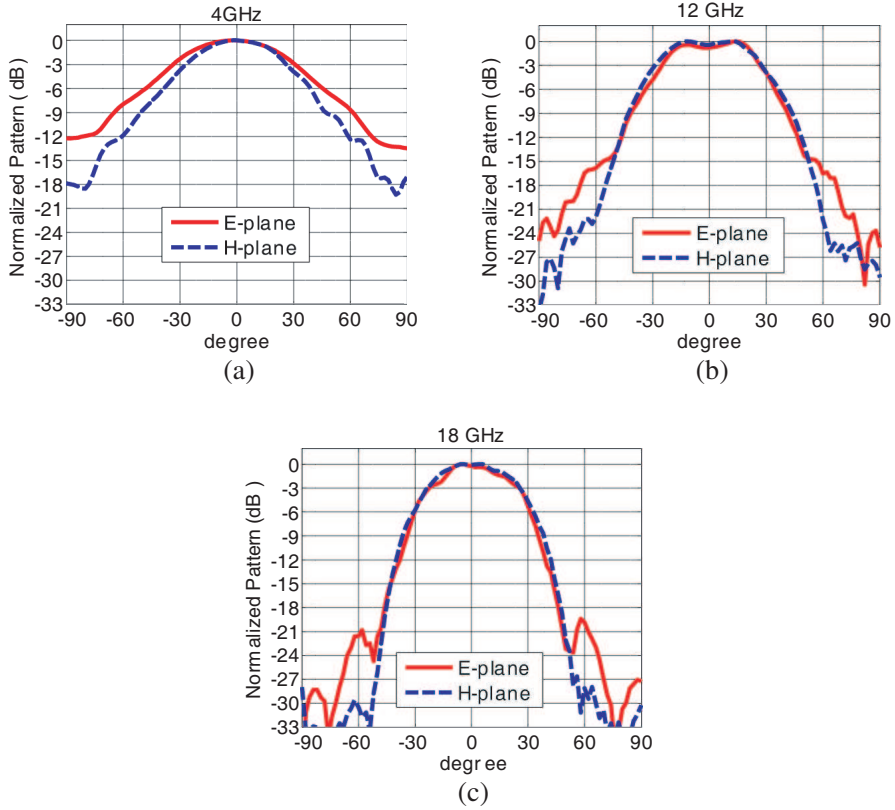


**Figure 12.** Measured *E*- and *H*-plane patterns of the dielectric-loaded horn at (a) 4 GHz, (b) 12 GHz, and (c) 18 GHz.

isolation is achieved, although the four metal arms are closely spaced at the feed to provide the dual polarization capability. As the antenna employs absorbers to obtain desirable radiation patterns, it is worth investigating the radiation efficiency ( $e$ ). For this, we used the following formulas:

$$e = \frac{G}{(1 - |\Gamma|^2) D} \quad (4)$$

$$\text{where } D \approx \frac{41000}{\theta_{-3\text{dB}}^E \theta_{-3\text{dB}}^H}. \quad (5)$$

Here,  $G$  and  $\Gamma$  in (4) refer to the measured realized gain (in dBi) and reflection coefficient. Also, the directivity  $D$  in (5) is calculated

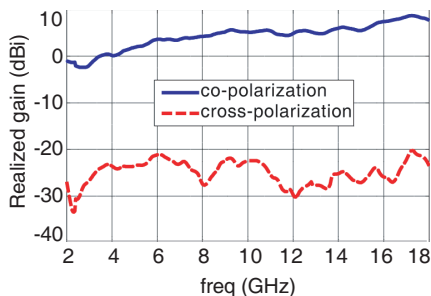


**Figure 13.** Measured co- and cross-pol gains of the dielectric-loaded horn antenna.

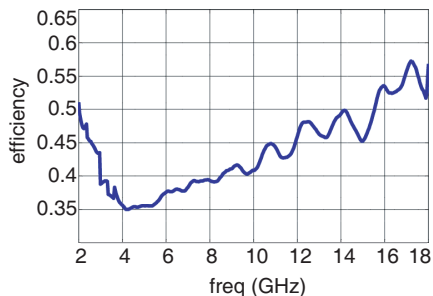


**Figure 14.** Radiation efficiency calculated from the measured parameters.

from the measured HPBW of  $E$ - and  $H$ -planes,  $\theta_{-3\text{dB}}^E$  and  $\theta_{-3\text{dB}}^H$ . Fig. 14 depicts the radiation efficiency of the dielectric-loaded horn. It varies from 35 to 57% and linearly grows after 4 GHz. The increase of efficiency below 4 GHz is due to the relatively broad HPBW and low gain (see Figs. 11 and 13). Moreover, the transition shown in Fig. 14 implies that there are two different radiation sources: 1) Below 4 GHz, the radiation is mainly from the metal arms, 2) above 4 GHz, the major radiation source is the guided wave inside the dielectric body.

## 6. CONCLUSION

We presented a new type of dielectric-loaded horn antenna providing stable radiation characteristics over 4–18 GHz. In contrast to metallic antennas such as double-ridged horns, the use of low-loss dielectric as a guiding structure enables the new antenna to produce broad far-field patterns in a wide bandwidth. Considerations to determine geometric and electric parameters of the antenna were discussed, particularly for curve and lens profiles closely related to the antenna's HPBW. We also described the antenna shielding structure by means of absorbers and conductive enclosure. The measured data of the final design demonstrate low return loss ( $< -10$  dB), large co- and cross-pol isolation ( $> 23$  dB) and broad HPBW ( $> 45^\circ$ ). These optimal characteristics are suitable for uniformly illuminating reflectors or test objects in electromagnetic test ranges. Moreover, considerable reduction in testing time can be expected thanks to the UWB operation, dual-polarization capability, and similar  $E$ - and  $H$ -plane patterns.

## REFERENCES

1. Walton, K. L. and V. C. Sundberg, "Broadband ridged horn design," *Microwave Journal*, Vol. 4, No. 2, 96–101, 1964.
2. Kerr, J. L., "Short axial length broad-band horns," *IEEE Trans. Antennas Propag.*, Vol. 21, No. 5, 710–714, 1973.
3. Burns, C., P. Leuchtman, and R. Vahldieck, "Analysis and simulation of a 1–18-GHz broadband double-ridged horn antenna," *IEEE Trans. Electromagn. Compat.*, Vol. 45, No. 1, 55–60, 2003.
4. Rodriguez, V., "New broadband EMC double-ridged guide horn antenna," *R. F. Des.*, Vol. 27, No. 5, 44–47, 2004.
5. Dehdasht-Heydari, R., H. R. Hassani, and A. R. Mallahzadeh, "A new 2–18 GHz quad-ridged horn antenna," *Progress In Electromagnetics Research*, PIER 81, 183–195, 2008.
6. Shen, Z. and C. Feng, "A new dual-polarized broadband horn antenna," *IEEE Antennas Wireless Propag. Lett.*, Vol. 4, 270–273, 2005.
7. Salema, C., C. Fernandes, and R. K. Jha, *Solid Dielectric Horn Antennas*, Artech House, Boston, 1998.
8. Olver, A. D., P. J. B. Clarricoats, A. A. Kishk, and L. Shafai, *Microwave Horns and Feeds*, IEE Press, London, 1994.
9. Lee, K. H, C. C. Chen, and R. Lee, "UWB dual-linear polarization dielectric horn antennas as reflector feeds," *IEEE Trans. Antennas Propag.*, Vol. 55, No. 3, 798–804, 2007.
10. Yaghjian, A. D. and E. T. Kornhauser, "A modal analysis of the dielectric rod antenna excited by HE<sub>11</sub> mode," *IEEE Trans. Antennas Propag.*, Vol. 20, No. 2, 122–128, 1972.
11. Lier, E., "A dielectric hybrid mode antenna feed: A simple alternative to the corrugated horn," *IEEE Trans. Antennas Propag.*, Vol. 34, No. 1, 21–29, 1986.
12. Duncan, F. W. and V. P. Minerva, "100 : 1 bandwidth balun transformer," *Proc. IRE*, Vol. 48, No. 2, 156–164, 1960.
13. Chang, L. C. T. and W. D. Burnside, "An ultrawide-bandwidth tapered resistive TEM horn antenna," *IEEE Trans. Antennas Propag.*, Vol. 48, No. 12, 1848–1857, 2000.
14. Lee, S. and H. Choi, "Design of an exponentially tapered TEM horn antenna for the wide broadband communication," *Microwave and Optical Tech. Lett.*, Vol. 40, No. 6, 531–534, 2004.
15. Yngvesson, K. S., D. H. Schaubert, T. L. Korzeniowski, E. L. Kollberg, T. Thungren, and J. F. Johansson, "Endfire

- tapered slot antennas on dielectric substrates," *IEEE Trans. Antennas Propag.*, Vol. 33, No. 12, 1392–1400, 1985.
16. Gazit, E., "Improved design of the Vivaldi antenna," *Proc. IEE Microwaves Antennas Propag., Ser. H*, Vol. 135, No. 2, 89–92, 1988.
  17. Shin, J. and D. H. Schaubert, "A parameter study of stripline-fed Vivaldi notch-antenna arrays," *IEEE Trans. Antennas Propag.*, Vol. 47, No. 5, 879–886, 1999.
  18. Lee, J. J., "Lens antennas," *Antenna Handbook Theory Applications and Design*, Y. T. Lo and S. W. Lee (eds.), Van Nostrand, New York, 1988.
  19. Bauerle, R. J., R. Schrimpf, E. Gyorko, and J. Henderson, "The use of a dielectric lens to improve the efficiency of a dual-polarized quad-ridge horn from 5 to 15 GHz," *IEEE Trans. Antennas and Propag.*, Vol. 57, No. 6, 1822–1825, 2009.
  20. Lai, A. K. Y., A. L. Sinopoli, and W. D. Burnside, "A novel antenna for ultra-wide-band applications," *IEEE Trans. Antennas Propag.*, Vol. 40, No. 7, 755–760, 1992.
  21. Clarricoats, P. J. B. and C. Salema, "Influence of the launching horn on the radiation characteristics of a dielectric cone feed," *Electronics Lett.*, Vol. 8, No. 8, 200–202, 1972.
  22. Salema, C., C. Fernandes, A. Martins, and J. Costa, "Radiation patterns of shielded dielectric horns: Analytical versus simulation approaches," *Proc. Conf. Telecommun.*, 47–51, Portugal, 2001.